



HAL
open science

Influence of the PuO₂ content on the sintering behaviour of UO₂-PuO₂ freeze-granulated powders under reducing conditions

Julie Simeon, Florent Lebreton, Laure Ramond, Nicolas Clavier, Guillaume Bernard-Granger

► To cite this version:

Julie Simeon, Florent Lebreton, Laure Ramond, Nicolas Clavier, Guillaume Bernard-Granger. Influence of the PuO₂ content on the sintering behaviour of UO₂-PuO₂ freeze-granulated powders under reducing conditions. *Journal of the European Ceramic Society*, 2021, 41 (13), pp.6778-6783. 10.1016/j.jeurceramsoc.2021.06.032 . cea-03550882

HAL Id: cea-03550882

<https://cea.hal.science/cea-03550882>

Submitted on 1 Feb 2022

HAL is a multi-disciplinary open access archive for the deposit and dissemination of scientific research documents, whether they are published or not. The documents may come from teaching and research institutions in France or abroad, or from public or private research centers.

L'archive ouverte pluridisciplinaire **HAL**, est destinée au dépôt et à la diffusion de documents scientifiques de niveau recherche, publiés ou non, émanant des établissements d'enseignement et de recherche français ou étrangers, des laboratoires publics ou privés.



Distributed under a Creative Commons Attribution - NonCommercial - NoDerivatives 4.0 International License

6/22/2021

1
2
3
4
5
6
7
8
9
10
11
12
13
14
15
16
17
18
19
20
21
22
23
24
25
26
27
28
29
30
31
32
33
34
35
36
37
38
39
40
41
42
43
44
45
46
47
48
49
50
51
52
53
54
55
56
57
58
59
60
61
62
63
64
65

Influence of the PuO₂ content on the sintering behaviour of UO₂-PuO₂ freeze-granulated powders under reducing conditions

Julie Simeon*, Florent Lebreton*, Laure Ramond*, Nicolas Clavier[‡] &
Guillaume Bernard-Granger*

*CEA, DES, ISEC, DMRC, Univ Montpellier, Marcoule France

[‡]ICSM, Univ Montpellier, CEA, CNRS, ENSCM, Bagnols-sur-Cèze, France

Abstract

The sintering behaviour of freeze-granulated UO₂-PuO₂ powders containing 33 and 15 mol% Pu/(U+Pu) was investigated under reducing conditions up to 1700 °C. For both compositions, the “grain size versus relative density” trajectory was constructed. All the experimental points form a single trajectory meaning that a relative density/grain size pair obtained after sintering seems independent of the thermal path (heating rate, soak time, soak temperature) and of the Pu content. Exploiting the “grain size versus relative density trajectory” enabled also to propose that densification was controlled by grain boundary diffusion and grain growth by the grain boundaries whatever the Pu content. An activation energy around 510 kJ/mol was obtained for densification, which was close to the value reported for the grain boundary diffusion of plutonium cations in U_{1-x}Pu_xO₂ polycrystals. Whatever the Pu/(U+Pu) content, the sintered microstructure of 98% dense samples possesses a homogeneous distribution of plutonium and uranium cations.

Keywords: Sintering; ceramics; oxides; microstructure; MOX

The submitted paper is original and has not been or is not being submitted to the peer review process to any other journal

*Corresponding author: guillaume.bernard-granger@cea.fr

1. Introduction

MOX fuel pellets ($\text{UO}_2\text{-PuO}_2$, cylinders with diameter and height typically around 10 mm) are manufactured by a dry-route powder metallurgy approach (grinding, pressing and sintering). Recently, the freeze-granulation of high-solid-loading water-based suspensions was shown to be a cutting-edge step to manufacture dense (relative density higher than 95%) MOX fuel pellets with a homogeneous distribution of the uranium and plutonium cations [1-3].

In a previous paper [3], the sintering behaviour of a freeze-granulated powder containing 15 mol% of Pu/(U+Pu) was investigated under reducing conditions (oxygen potential of -468 kJ/mol at 1700 °C) in order to target a O/M ratio of 1.96, which is a strict specification to be respected for fuel dedicated to fast neutron nuclear reactors. Thereby, the present short communication focuses on sintering experiments performed on a freeze-granulated powder containing 33 mol% of Pu/(U+Pu) under reducing conditions targeting the same O/M ratio. The results are then compared to the ones already reported for the 15 mol% Pu/(U+Pu) powder [3].

2. Experimental section

A freeze-granulated powder containing 33 mol% Pu/(U+Pu) was elaborated by the same route as the one retained for the powder containing 15 mol% Pu/(U+Pu) [1, 3]. The UO_2 raw powder was synthesized through a dry route by reduction of UF_6 in gas phase. It contains 8.5 wt% of the U_3O_8 phase and has a global overall O/M ratio of 2.20. The PuO_2 powder was obtained through oxalic precipitation of plutonium (IV) nitrate and calcination in air. Its O/M ratio is 2.00.

As shown in the supplementary material and as already reported for the freeze-granulated powder containing 15 mol% Pu/(U+Pu) [3], the individual granules constituting the 33 mol% Pu/(U+Pu) powder, observed using SEM (scanning

1
2
3
4
5
6
7
8
9
10
11
12
13
14
15
16
17
18
19
20
21
22
23
24
25
26
27
28
29
30
31
32
33
34
35
36
37
38
39
40
41
42
43
44
45
46
47
48
49
50
51
52
53
54
55
56
57
58
59
60
61
62
63
64
65

electron microscopy, Supra 55 VP, Zeiss), have a spherical shape and are devoid of any central cavities. Using microscopy observations, the cumulative number frequency distribution of the granule-size for both powders was also determined (see also supplementary material). The number median diameters ($D_n(50)$) are around 65 and 130 μm for the 15 and 33 mol% Pu/(U+Pu) powders, respectively. Using thermal ionization mass spectrometry (TIMS, VG-54 magnetic sector mass spectrometer, Isotopx), the obtained Pu/(U+Pu) contents in the freeze-granulated powders were determined to be $14.4(\pm 0.4)$ and $32.1(\pm 0.3)$ mol%.

As for the 15 mol% Pu/ (U+Pu) powder [3], cylindrical samples (diameter of 5.4 mm and a height around 6-7 mm) were obtained by uniaxial pressing of the 33 mol% Pu/(U+Pu) freeze-granulated powder with a compaction pressure set to 450 MPa (manual hydraulic press, Atlas 25, Specac). By taking a theoretical volume mass of 11.0 g/cm^3 at room temperature whatever the Pu/(U+Pu) content (calculated, as already explained in a previous paper with some limitations to consider [3], using the relationship established by Philipponneau [4], stating that $\text{U}_{1-y}\text{Pu}_y\text{O}_{2-x}$ solid solutions have a fluorite structure, specifying that the target O/M ratio is 1.96 and assuming a molar mass of 238 g for U/Pu), the relative green density was around $58(\pm 0.4)\%$ for the 33 mol% Pu(U+Pu) green samples against $57(\pm 0.4)\%$ for the 15 mol% Pu/(U+Pu) ones.

As justified previously [3], all samples were exposed at 600 °C for 2 h in an Ar/4 vol% H₂ atmosphere humidified with 1200 vpm of water (oxygen partial pressure and oxygen potential set to 1.3×10^{-27} bar and -450 kJ/mol at 600 °C, respectively) for a debinding step. Such a treatment has potentially an influence on the O/M ratio of the starting UO₂ powder [3].

The green pellets were sintered from room temperature up to 1700 °C in a high temperature dilatometer (DIL402C, Netzsch) under Ar/4 vol% H₂. According to

1 Kato, the oxygen partial pressure required to obtain an O/M ratio around 1.96
 2 for a MOX composition containing 32.1 mol% Pu/(U+Pu), at 1700 °C, is around
 3
 4 1.2×10^{-11} bar, which gives an oxygen potential of -413 kJ/mol [3, 5]. In
 5
 6 comparison, for the same temperature and the same O/M value, the oxygen
 7
 8 partial pressure and the oxygen potential were 4.1×10^{-13} bar and -468 kJ/mol,
 9
 10 respectively, for sintering the green samples containing 14.4 mol% Pu/(U+Pu)
 11
 12 [3]. Thereby, the atmosphere was monitored and controlled with an oxygen
 13
 14 pump (Gen'air, Setnag) in order to have a constant water vapour concentration
 15
 16 of 550 vpm (calculated using the Wheeler approach [6] to obtain the target
 17
 18 oxygen partial pressure and oxygen potential at 1700 °C) during the sintering
 19
 20 runs of the 33 mol% Pu/(U+Pu) samples. For comparison, the water vapour
 21
 22 concentration was adjusted to 100 vpm for sintering the 15 mol% Pu/(U+Pu)
 23
 24 pellets [3].
 25
 26
 27

28 Heating rates fixed to 2, 3 and 4 °C/min were used for the sintering runs. The
 29
 30 isothermal duration was ranging from 0 to 4h and the target temperature from
 31
 32 1550 to 1700 °C. The equipment contribution was subtracted based on a blank
 33
 34 measurement made with an Al₂O₃ reference.
 35
 36
 37

38 As reported before, the following relation is used to investigate densification [1-
 39
 40 3, 7-8]:
 41
 42
 43

$$44 \quad D_{(T)}(\%) = D_0 \frac{1}{\xi^2 \left[1 + \frac{\Delta L_{(T)}}{L_0}\right]^3} e^{3\alpha(T-T_0)} \quad (1)$$

45
 46
 47
 48
 49
 50 where: $D_{(T)}$ is the sample instantaneous relative density, D_0 is the sample relative
 51
 52 green density, ξ represents the shrinkage anisotropy of the sample and is given
 53
 54 by $\xi = \frac{\phi_f L_0}{\phi_0 L_f} = \frac{\phi_{(T)} L_0}{\phi_0 L_{(T)}}$ with ϕ_f the final diameter, L_f the final height, ϕ_0 the
 55
 56 initial diameter, L_0 the initial height, $\phi_{(T)}$ the instantaneous diameter and $L_{(T)}$
 57
 58 the instantaneous height, $\Delta L_{(T)} = L_{(T)} - L_0$ (<0) is the sample height variation,
 59
 60
 61
 62
 63
 64
 65

1 α is the linear thermal expansion coefficient, T is the instantaneous absolute
2 temperature and T_0 the absolute room temperature. From a practical point of
3 view, α is determined from the cooling steps of the dilatometer runs. An average
4 value of $10.5(\pm 0.2) \times 10^{-6}$ is retained for the 33 mol% Pu/(U+Pu) samples against
5
6 value of $11.6(\pm 0.6) \times 10^{-6}$ for the 15 mol% Pu/(U+Pu) pellets. For all the sintering runs
7
8 the parameter ξ was close to 1.
9
10

11
12
13
14 The density of the sintered samples was measured using the Archimedes method
15 with bromobenzene (dry, immersed and humid weights, three series of
16 measurements were carried out for each sample).
17
18
19
20

21
22 The average grain size of the different green and sintered samples was
23 investigated. For green compacts, it was determined from fracture surfaces
24 observed using SEM (Supra 55 VP, Zeiss) in secondary electron mode. For
25 sintered samples, each complete sample was embedded in a resin and a mirror
26 longitudinal polished cross section was prepared, including a final
27 mechanical-polishing step using 250 and 40 nm colloidal silica suspensions. For
28 the 15 mol% Pu/(U+Pu) samples, such a protocol was enough to reveal the
29 grains of the polycrystals using the backscattered electron mode during SEM
30 (Mira 3, Tescan) observations [3]. For the 33 mol% Pu/(U+Pu), it was not as
31 effective and the grain size was obtained from IPF (inverse pole figure) maps
32 collected by EBSD (electron backscatter diffraction). For all samples, the
33 average grain size was determined by the line-intercept method (at least 300
34 grains are considered, correction factor set to 1.56 [9]) from SEM images and
35 IPF maps.
36
37
38
39
40
41
42
43
44
45
46
47
48
49
50

51
52 Polished cross sections from the 33 and 15 mol% Pu/(U+Pu) samples sintered
53 for 4 h at 1700 °C (heating rate fixed to 2 °C/min, almost 98% dense samples
54 with similar grain sizes) were characterized by wavelength dispersive X-ray
55 spectroscopy (WDS) using an electron probe micro-analyser (EPMA, SX100,
56
57
58
59
60
61
62
63
64
65

1 Cameca). On each pellet, uranium and plutonium mappings were collected on
2 several $1024\ \mu\text{m}\times 1024\ \mu\text{m}$ areas. Measurements were performed at 20 kV at the
3 U-M_α and Pu-M_β lines. In these conditions, the probe volume is about $0.7\ \mu\text{m}$ in
4 diameter and $0.5\ \mu\text{m}$ in depth. U and Pu line intensity mappings were collected
5 on at least three areas ($1024\ \mu\text{m}\times 1024\ \mu\text{m}$ with a $1\ \mu\text{m}$ step) randomly located
6 on the samples. The different mappings gave very similar results. These
7 measurements were completed by quantitative measurements on several 500
8 μm -long lines (with a $1\ \mu\text{m}$ step), each one located inside one of the mappings.
9 For the latter, the U and Pu contents were quantified by applying the ZAF
10 method and using UO_2 and PuO_2 samples as standards for U, Pu (and O), with
11 an uncertainty of about 1 wt% on the U and Pu contents measured at each point.
12 The comparison between the distribution of counts number in mappings and that
13 of Pu content in the quantitative lines allowed pseudo-quantitative mappings to
14 be created.

31 3. Results and discussion

32 Fig. 1a shows the increase in relative density as a function of the temperature
33 for both kinds of samples. Whatever the heating rate and the $\text{Pu}/(\text{U}+\text{Pu})$ content,
34 samples start to densify around $650\ ^\circ\text{C}$. The lower the heating rate, the higher
35 the relative density for a given temperature and $\text{Pu}/(\text{U}+\text{Pu})$ content. As already
36 explained in the literature, the lower the heating rate, the longer the exposure
37 time and the higher the shrinkage and relative density reached at a given
38 temperature [2-3, 7-8, 10]. More interestingly, and even if the green densities
39 are not exactly the same (difference of 1%), the 33 mol% $\text{Pu}/(\text{U}+\text{Pu})$ samples
40 reach higher relative density values (4-6% of difference), whatever the heating
41 rate applied. Accordingly, a higher $\text{Pu}/(\text{U}+\text{Pu})$ content promotes densification
42 during the heating step of the sintering runs, as previously reported by Kutty
43 [11].

As shown on Fig. 1b, the gain in relative density during the soak period (4h) at 1700 °C for samples heated at 2 °C/min is much higher (around 12% against 5%) for the 15 mol% Pu/(U+Pu) sample. Then, even if a larger Pu content is beneficial during heating, the difference between both kinds of sample collapses during the soak period. Moreover, the final relative density reached by the sample containing 15 mol% Pu/(U + Pu) is ultimately slightly greater at the end of the plateau.

Fig. 1c shows the densification rate as a function of temperature for both kind of samples. Whatever the Pu/(U+Pu) content, the higher the heating rate, the higher the instantaneous densification rate for a given temperature. This trend has been already reported for radioactive and non-radioactive oxides [2, 7-8]. For the 15 mol% Pu/(U+Pu) samples, the curves do not exhibit the traditional bell-shape with a clear maximum densification rate, because of the limitation in the maximum temperature achievable. Similar results have been obtained by Kutty [11] and Nakamichi [12]. Conversely, a bell shape curve is observed for the 33 mol% Pu/(U+Pu) samples, confirming an easier densification during the heating step of the runs. For these samples, the higher the heating rate, the higher the temperature at the maximum densification rate: 1580 °C for 2 °C/min, 1590 °C for 3 °C/min and 1635 °C for 4 °C/min.

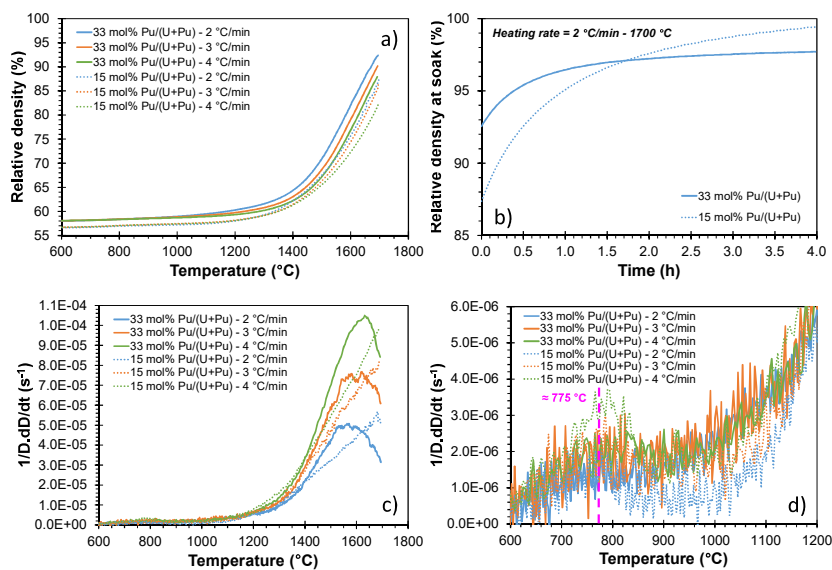


Figure 1

1 The fact that densification is favored during the heating step when the
2 Pu/(U+Pu) content increases is also possibly linked to the fact that sintering is
3 carried out in a reducing atmosphere for both kinds of samples (a similar O/M
4 ratio of 1.96 is targeted). It can therefore be envisaged that the higher the Pu
5 content in the samples, the greater the proportion of plutonium in the +III
6 oxidation state and possibly counterbalanced by the creation of point defects to
7 achieve electroneutrality, which will promote densification.
8
9
10
11
12
13
14
15

16 Fig. 1d shows a zoom of Fig. 1c in the 600-1200 °C temperature range.
17 Whatever the heating rate and the Pu content, the instantaneous densification
18 rate exhibits a first maximum value around 775 °C. It means that densification
19 starts around 600 °C and slows-down from 775 °C. As postulated in previous
20 papers [2-3], in agreement with similar results reported in the literature [11, 13-
21 14], and even if additional tests are needed for validation (X-ray diffraction
22 experiments as a function of temperature and time, as reported for example
23 recently by Vauchy [19], or transmission electron microscopy investigations at
24 the LECA-STAR facility in CEA Cadarache on interrupted sintered samples),
25 we postulate that a solid solution forms in the densifying samples around 775
26 °C, whatever the heating rate value and the Pu content. As stated before [3],
27 because the solid solution formation implies the interdiffusion of Pu cations into
28 the UO₂ lattice and U cations into the PuO₂ lattice, it provokes a decrease of the
29 densification rate. Even if we have no formal proof to date, we understand
30 intuitively that the atomic movements involved during the step of forming a
31 grain of solid solution from a grain of UO₂ and a grain of PuO₂ are favoured
32 compared to those allowing the closure of the intergranular porosity due to
33 strong gradients of chemical potentials which will be at the origin of the
34 interdiffusion on short distances. Whatever the Pu content, when densification
35 resumes around 900-1000°C, the samples are possibly more homogeneous and
36 could be described as a polycrystalline body constituted by grains of U_{1-y}Pu_yO_{2-x}
37 solid solutions and pores, rather than UO₂ and PuO₂ grains alone.
38
39
40
41
42
43
44
45
46
47
48
49
50
51
52
53
54
55
56
57
58
59
60
61
62
63
64
65

The “grain size versus relative density” trajectory was then constructed from the relative density and grain size values obtained for the different samples. As shown on Fig. 2, it is critical to point out that, as a first approximation due to the magnitude of the error bars and even if the dataset for the 33 mol% Pu/(U+Pu) composition is systematically slightly above the one of the 15 mol% Pu/(U+Pu) formulation, all the experimental points seem to form a single trajectory (dashed black curve, first level fitting using the Lab Fit Curve Fitting software), meaning that a relative density/grain size pair obtained after sintering seems independent of the thermal path (heating rate, soak time, soak temperature) and of the Pu content. If it is well established that a multitude of sintering experimental conditions led to the same microstructure, as previously reported for radioactive and non-radioactive oxides [2-3, 7-8], such an observation had so far never been reported in the literature regarding the Pu content for MOX fuels.

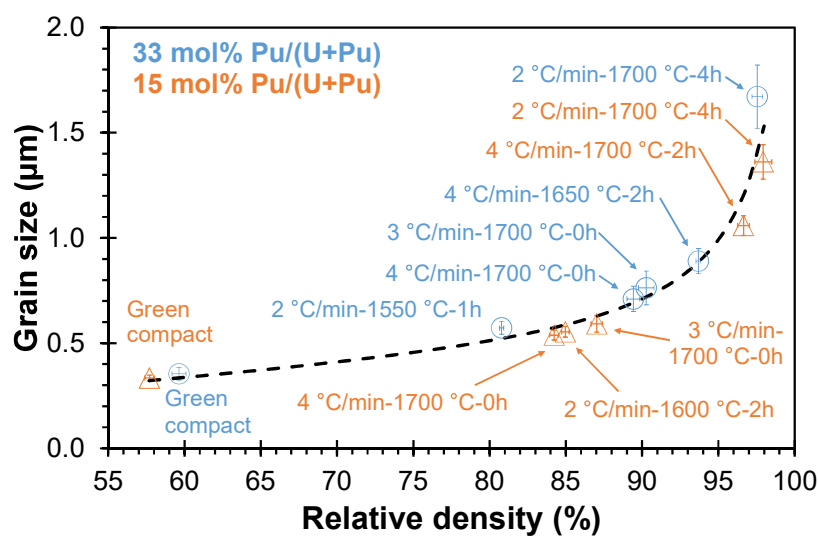


Figure 2

Always as a first approximation, neglecting the tiny difference of the datasets between the 15 and 33 mol% Pu/(U+Pu) samples, the relative density/grain size pairs constituting the sintering trajectory shown on Fig. 2 were then fitted with theoretical expressions linking the grain size to the relative density [15]. The best coefficient of determination value amongst these fits is obtained when grain growth is controlled by the grain boundaries and densification is controlled by

grain boundary diffusion, as shown on Fig. 3, independently of the Pu/(U+Pu) content. Nonetheless, other mechanism combinations lead to coefficient of determination values above 0.95.

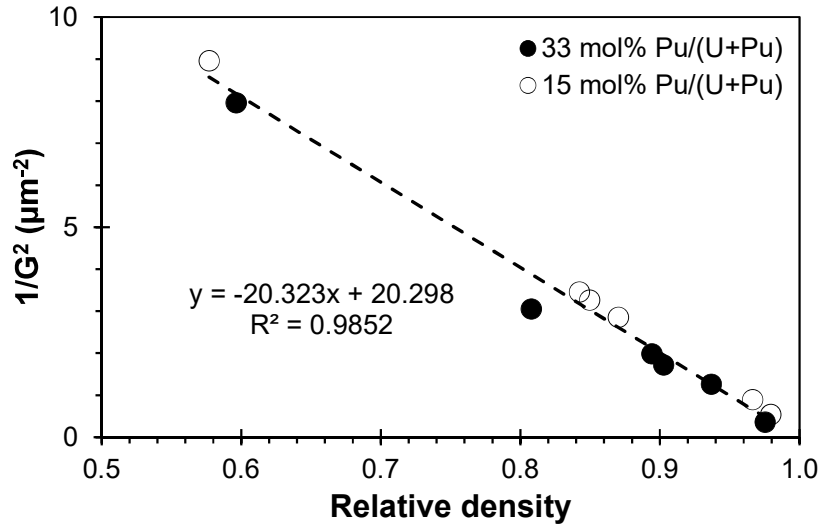


Figure 3

As demonstrated in a previous paper [15], we have:

$$\frac{\gamma_b D_b^\perp}{50\alpha\gamma_{sv}\delta_b^2 D_b} = 20.323 \approx 20 \mu\text{m}^{-2} \quad (2)$$

where γ_b is the grain boundary surface tension, D_b^\perp is the matter diffusion coefficient through the grain boundaries, α is a constant proportionality factor between the grain size G and the radius of curvature ρ of the grain boundaries, γ_{sv} is the solid/vapour surface tension, δ_b is the grain boundary thickness and D_b is the grain boundary diffusion coefficient. Assuming that, $\gamma_{sv} \approx 2\gamma_b$, $\alpha \approx 2$ [20] and a typical value of 1 nm for δ_b , it is found that:

$$D_b \approx 250D_b^\perp \quad (3)$$

Accordingly, the diffusion coefficient along the grain boundaries appears to be much higher than the one through the grain boundaries. This could explain why

1 grain growth appears limited during sintering both compositions investigated
 2 despite a maximum temperature as high as 1700 °C. Such a behaviour could be
 3 attributable to a homogeneous distribution of the pores and to a control of their
 4 size in the raw samples, due to the preparation of the powders that are shaped
 5 by uniaxial pressing by the freeze-granulation route. To confirm this hypothesis,
 6 mercury porosimetry could be used. Unfortunately, this method of
 7 characterization is not available in our nuclearized glove boxes allowing to work
 8 with plutiferous material. In addition, even if the possibility of carrying out
 9 this type of analysis would then arise the problem of the outlet of the analysed
 10 materials.

11
 12 In order to give more strength to the mechanisms proposed for the control of
 13 densification and grain growth, let us determine the apparent activation energy
 14 for the mechanism controlling densification. As perfectly established now, the
 15 equation for the densification rate can be separated into temperature-dependent,
 16 grain size-dependent and density-dependent quantities to be rearranged as [8,
 17 16-17]:

$$18 \quad \ln \left[T \frac{dD}{dT} \frac{dT}{dt} \right] = - \frac{Q_d}{RT} + \ln\{F[D]\} + \ln(A) - n \ln(G) \quad (4)$$

19 where A is a constant, $F[D]$ is a function of density only, Q_d is the apparent
 20 activation energy for the mechanism controlling densification, R is the universal
 21 gas constant, T is the absolute temperature, G is the grain size, n is the grain size
 22 exponent whose value depends on whether the densification rate is controlled
 23 by lattice diffusion ($n = 3$) or grain-boundary diffusion ($n = 4$) and dT/dt is the
 24 heating rate that is held constant during anisothermal sintering experiments.

25
 26 A plot of the left-hand side of relation (4) versus $1/T$ would give a value for Q_d
 27 provided that the data points are taken at a constant value of D and G . Fig. 2
 28 shows that each value of relative density corresponds to a single value of grain
 29

size, regardless of the sintering conditions and of the Pu content. Then, points for a constant value of D are generated by changing the heating rate. The measurements led to values of Q_d at different values of D . This formalism is known as the Constant Rates of Heating method.

Using such an approach leads to Fig. 4. The apparent activation energy determined for the 33 mol% Pu/(U+Pu) samples is 490 ± 60 kJ/mol, against 530 ± 10 kJ/mol for the 15 mol% Pu/(U+Pu) ones. Thereby, in a first approximation, an apparent average activation energy of 510 ± 50 kJ/mol, associated with the densification mechanism, is then calculated whatever the Pu content.

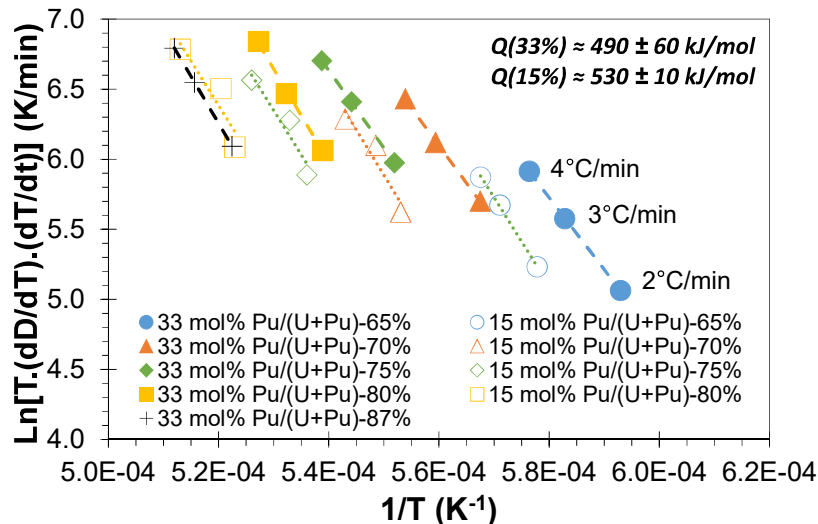


Figure 4

It has to be emphasized that the uncertainty related to the activation energy value of the 33 mol% Pu/(U+Pu) composition is substantially higher. Looking more closely at Fig. 4, it seems that for the 15 mol% Pu/(U + Pu) composition all slopes allowing access to the value of the activation energy are really similar. This is not the case for the 33 mol% Pu/(U + Pu) composition where the slope seems to increase, at least when going from 65 to 75% relative density. However, this apparent difference in behaviour may be related only to the data acquisition phase on the dilatometer. Indeed, for an imposed heating rate, we do

not have scrupulously the same value of relative density reached for a given temperature, especially for the 33 mol% Pu/(U+Pu) samples.

Noyau measured the volume and grain boundary diffusion coefficients of plutonium cations in an $U_{0.55}Pu_{0.45}O_{2-x}$ polycrystalline material, for an oxygen potential set to -395 kJ/mol [18]. He reported an activation energy for the grain boundary diffusion of plutonium cations around 506 kJ/mol [18]. It is very close to the one we obtained from our sintering experiments. Accordingly, we postulate that densification of our different samples during sintering is controlled by the grain boundary diffusion of the plutonium cations, whatever the Pu content, which is consistent with the abovementioned densification/grain growth scenario.

At this stage, an additional remark must be reported. In a separate paper [2], sintering investigations of a UO_2 - PuO_2 powder, containing 11 wt% of PuO_2 and also synthesized by freeze-granulation, were completed also at temperatures up to 1700 °C. An activation energy around 630 kJ/mol was obtained for densification [2], which was close to the value reported for volume diffusion of plutonium cations in $U_{1-x}Pu_xO_2$ polycrystals [18]. For these investigations, the UO_2 raw powder used was synthesized through a liquid route from uranyl nitrate solution. In the present paper, the UO_2 raw powder was synthesized through a dry route by reduction of UF_6 in gas phase (it contains also 8.5 wt% of the U_3O_8 phase). We cannot therefore exclude a possible influence of the type of UO_2 powder selected on the mechanism controlling densification during sintering. A more important difference should however be underlined. The oxygen potential imposed at 1700 °C was -389 kJ/mol for the sintering tests carried out on the formulation containing 11wt% PuO_2 reported in a separate paper [2]. In the present article, the oxygen potential imposed at 1700 °C was -413 and -468 kJ/mol for the 33 and 15 mol% Pu/(U+Pu) samples, respectively. Therefore, it seems more probable that it is the difference in partial pressure of oxygen

imposed during the sintering runs at high temperature which is at the origin of a different densification mechanism.

Polished cross sections from the 33 and 15 mol% Pu/(U+Pu) samples sintered for 4 h at 1700 °C (heating rate fixed to 2 °C/min, almost 98% dense samples with a similar grain size) were characterized by WDS/EPMA analyses. The resulting Pu mappings in Fig. 5 show that the Pu distribution inside the 33 mol% Pu/(U+Pu) pellet is not as homogeneous as in the 15 mol% one, but remains nonetheless quite homogeneous.

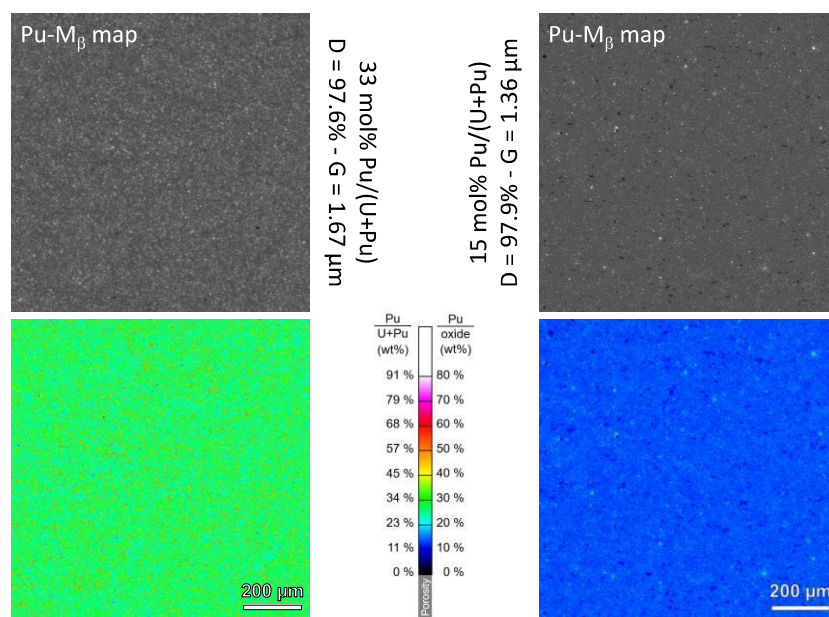


Figure 5

Notably, neither UO_2 nor Pu-rich large clusters are observed in the pellets, whatever their average Pu content. The Pu-rich clusters observed are just a few micrometres in size, with Pu/(U+Pu) ratios only very locally exceeding 50 mol%. It confirms that the freeze-granulation route of high-solid-loading water-based suspensions is a suitable route to manufacture dense and homogeneous MOX fuel pellets even for Pu/(U+Pu) contents as high as 33 mol%.

4. Conclusion

1 The sintering behaviour of a MOX ($\text{UO}_2\text{-PuO}_2$) freeze-granulated powder
2 containing 33 mol% Pu/(U+Pu) has been investigated under reducing conditions
3 and compared to what had been obtained in a previous study on a powder
4 prepared in the same way but containing only 15 mol% Pu/(U+Pu).
5
6
7
8
9

10
11 It was shown that the “grain size versus relative” density trajectory seems
12 independent of the Pu/(U+Pu) content. Likewise, regardless of the Pu/(U+Pu)
13 content, densification seems to be controlled by the grain boundary diffusion of
14 the plutonium cations and grain growth seems to be controlled by the grain
15 boundaries.
16
17
18
19
20
21
22

23
24 Finally, the freeze-granulation route of high-solid-loading water-based
25 suspensions has been shown to be a suitable route to manufacture dense and
26 homogeneous MOX fuel pellets even for Pu/(U+Pu) contents as high as 33
27 mol%.
28
29
30
31
32

33
34 Additional work is currently underway on a powder obtained by freeze-
35 granulation and another by direct advanced co-grinding, both integrating 26
36 mol% Pu/(U+Pu).
37
38
39
40

41
42 **Acknowledgements:** The authors warmly thank Mathilde Pons, Méghan
43 Alibert, Lise Barnouin, Camille Aloin and Romain Lauwerier, for their precious
44 help during the experiments carried out within the framework of this study.
45
46
47
48
49
50
51
52
53
54
55
56
57
58
59
60
61
62
63
64
65

References

1
2
3
4 [1] F. La Lumia, L. Ramond, C. Pagnoux, P. Coste, F. Lebreton, J.R. Sevilla, G.
5 Bernard-Granger. Dense and homogeneous MOX fuel pellets manufactured
6 using the freeze granulation route. J. Amer. Ceram. Soc. 103 (2020) 3020-3029.
7
8 <https://doi.org/10.1111/jace.17005>
9

10
11
12
13 [2] M. Le Guellec, F. Lebreton, L. Ramond, A. Ndiaye, T. Gervais, G. Bernard-
14 Granger. Sintering investigations of a UO₂-PuO₂ powder synthesized using the
15 freeze-granulation route. Scripta Mater. 186 (2020) 190-195.
16
17 <https://doi.org/10.1016/j.scriptamat.2020.05.036>
18
19

20
21
22
23 [3] J. Simeon, F. Lebreton, L. Ramond, F. La Lumia, N. Clavier, G. Bernard-
24 Granger. Sintering of a UO₂-PuO₂ freeze-granulated powder under reducing
25 Conditions. J. Eur. Ceram. Soc. 40 (2020) 5900-5908.
26
27 <https://doi.org/10.1016/j.jeurceramsoc.2020.07.022>
28
29

30
31
32
33 [4] R. Vauchy, A.C. Robisson, R.C. Belin, P.M. Martin, A.C. Scheinost, F.
34 Hodaj. Room temperature oxidation of hypostoichiometric uranium-plutonium
35 mixed oxides U_{1-y}Pu_yO_{2-x}. A depth-selective approach. J. Nucl. Mater. 465
36
37 (2015) 349-357. <https://doi.org/10.1016/j.jnucmat.2015.05.033>
38
39

40
41
42
43 [5] M. Kato, M. Watanabe, T. Matsumoto, S. Hirooka, M. Akashi. Oxygen
44 potentials, oxygen diffusion coefficients and defect equilibria of
45 nonstoichiometric of (U, Pu)O_{2±x}. J. Nucl. Mater. 487 (2017) 424-432.
46
47 <https://doi.org/10.1016/j.jnucmat.2017.01.056>
48
49

50
51
52
53 [6] V. J. Wheeler, I.G. Jones. Thermodynamic and composition changes in
54 UO_{2±x} (x < 0.005) at 1950 K. J. Nucl. Mater. 42 (1972) 117-121.
55
56 [https://doi.org/10.1016/0022-3115\(72\)90018-9](https://doi.org/10.1016/0022-3115(72)90018-9)
57
58
59

1 [7] G. Bernard-Granger, C. Guizard. Apparent activation energy for the
2 densification of a commercially available granulated zirconia powder. J. Amer.
3 Ceram. Soc. 90 (2007) 1246-1250. [https://doi.org/10.1111/j.1551-](https://doi.org/10.1111/j.1551-2916.2006.01415.x)
4 [2916.2006.01415.x](https://doi.org/10.1111/j.1551-2916.2006.01415.x)
5
6

7
8
9 [8] N. Benameur, G. Bernard-Granger, A. Addad, S. Raffy, C. Guizard.
10 Sintering analysis of a fine-grained alumina – magnesia spinel powder. J. Amer.
11 Ceram. Soc. 94 (2011) 1388-1396. [https://doi.org/10.1111/j.1551-](https://doi.org/10.1111/j.1551-2916.2010.04271.x)
12 [2916.2010.04271.x](https://doi.org/10.1111/j.1551-2916.2010.04271.x)
13
14
15
16

17
18
19 [9] M.I. Mendleson. Average grain size in polycrystalline ceramics. J. Amer.
20 Ceram. Soc. 52 (1969) 443-446. [https://doi.org/10.1111/j.1151-](https://doi.org/10.1111/j.1151-2916.1969.tb11975.x)
21 [2916.1969.tb11975.x](https://doi.org/10.1111/j.1151-2916.1969.tb11975.x)
22
23
24
25

26
27 [10] E. Sato, C.P. Carry. Yttria doping and sintering of submicrometer-grained
28 α -alumina. J. Amer. Ceram. Soc. 79 (1996) 2156-2160.
29 <https://doi.org/10.1111/j.1151-2916.1996.tb08950.x>
30
31
32
33
34
35

36 [11] T.R.G. Kutty, P.V. Hegde, K.B. Khan, S. Majumdar, D.S.C. Purushotham.
37 Sintering studies on $\text{UO}_2\text{-PuO}_2$ pellets with varying PuO_2 content using
38 dilatometry. J. Nucl. Mater. 282 (2000) 54-65. [https://doi.org/10.1016/S0022-](https://doi.org/10.1016/S0022-3115(00)00394-9)
39 [3115\(00\)00394-9](https://doi.org/10.1016/S0022-3115(00)00394-9)
40
41
42
43
44
45

46 [12] S. Nakamichi, S. Hirooka, M. Kato, T. Sunaoshi, A. T. Nelson, K. J.
47 McClellan. Effect of O/M ratio on sintering behavior of $(\text{Pu}_{0.3}\text{U}_{0.7})\text{O}_{2-x}$. J. Nucl.
48 Mater. 535 (2020) 152188. <https://doi.org/10.1016/j.jnucmat.2020.152188>
49
50
51
52
53

54 [13] R. Manzel, W.D. Dorr. Fabrication of $\text{UO}_2\text{-Gd}_2\text{O}_3$ fuel pellets. Ceram. Bull.
55 59 (1980) 601-616
56
57
58
59
60
61
62
63
64
65

1 [14] W. Dorr, S. Hellmann, G. Mages. Study of the formation of $\text{UO}_2\text{-PuO}_2$ solid
2 solution by means of $\text{UO}_2\text{-CeO}_2$ simulate. J. Nucl. Mater. 140 (1986) 7-10.
3 [https://doi.org/10.1016/0022-3115\(86\)90190-X](https://doi.org/10.1016/0022-3115(86)90190-X)
4
5

6
7 [15] G. Bernard-Granger, C. Guizard. New relationships between relative
8 density and grain size during solid-state sintering of ceramic powders. Acta
9 Mater. 56 (2008) 6273–6282. <https://doi.org/10.1016/j.actamat.2008.08.054>
10
11

12 [16] J. Wang, R. Raj. Activation energy for the sintering of two-phase alumina-
13 zirconia ceramics. J. Am. Ceram. Soc. 74 (1991) 1959–63.
14 <https://doi.org/10.1111/j.1151-2916.1991.tb07815.x>
15
16

17 [17] J.D. Hansen, R.P. Rusin, M.H. Teng, D.L. Johnson. Combined-stage
18 sintering model. J. Am. Ceram. Soc. 75 (1992) 1129–35.
19 <https://doi.org/10.1111/j.1151-2916.1992.tb05549.x>
20
21

22 [18] S. Noyau. Etude des phénomènes d'autodiffusion et d'interdiffusion du
23 plutonium dans les céramiques de type $\text{U}_{1-y}\text{Pu}_y\text{O}_{2\pm x}$. PhD Thesis, University of
24 Limoges, (2012)
25
26

27 [19] R. Vauchy, R.C. Belin, A.-C. Robisson, F. Hodaj. Effect of cooling rate on
28 achieving thermodynamic equilibrium in uranium-plutonium mixed-oxides. J.
29 Nucl. Mater. 469 (2016) 125-132.
30 <https://doi.org/10.1016/j.jnucmat.2015.11.049>
31
32

33 [20] D. Bernache-Assollant. Chimie-physique du frittage. Paris: Editions
34 Hermès, 1993.
35
36

Figure captions

1
2
3
4 Fig. 1: a) Relative density as a function of the temperature during the heating
5 step; b) Relative density as a function of the soak time at 1700 °C; c)
6
7
8
9
10
11
12
13
14
15
16
17
18
19
20
21
22
23
24
25
26
27
28
29
30
31
32
33
34
35
36
37
38
39
40
41
42
43
44
45
46
47
48
49
50
51
52
53
54
55
56
57
58
59
60
61
62
63
64
65

Densification rate as a function of the temperature; d) zoom of c) in the 600-1200 °C temperature range

Fig. 2: Grain size versus relative density trajectory. For each experimental point, the values given are the heating rate, the sintering temperature and the time spent at the sintering temperature

Fig. 3: Fitting of the experimental points of the grain size versus relative density trajectory for a scenario based on densification being controlled by grain boundary diffusion and grain growth by the grain boundaries

Fig. 4: Determination of the apparent activation energy for densification using the anisothermal Constant Rates of Heating method. For each dataset, the value given is the density at which the data was extracted from the three heating rate values

Fig. 5: Pu-M_β intensity mapping obtained by EPMA/WDS at 20 kV (arbitrary grey scales) and coloured pseudo-quantified Pu mapping for 98% dense samples having similar grain sizes

Supplementary material: a) SEM observations of some typical granules constituting the freeze-granulated powders containing 33 and 15 mol% Pu/(U+Pu); b) Cumulative number frequency of the individual granules constituting the freeze-granulated powders containing 33 and 15 mol% Pu/(U+Pu). The measurements were performed using optical microscopy observations of powder samples positioned on a glass coverslip. Each individual

granule projected area is measured and an equivalent two-dimensional disc diameter is calculated (no correction factor). Around 1000 granules are considered for each powder

1
2
3
4
5
6
7
8
9
10
11
12
13
14
15
16
17
18
19
20
21
22
23
24
25
26
27
28
29
30
31
32
33
34
35
36
37
38
39
40
41
42
43
44
45
46
47
48
49
50
51
52
53
54
55
56
57
58
59
60
61
62
63
64
65

Figure 1

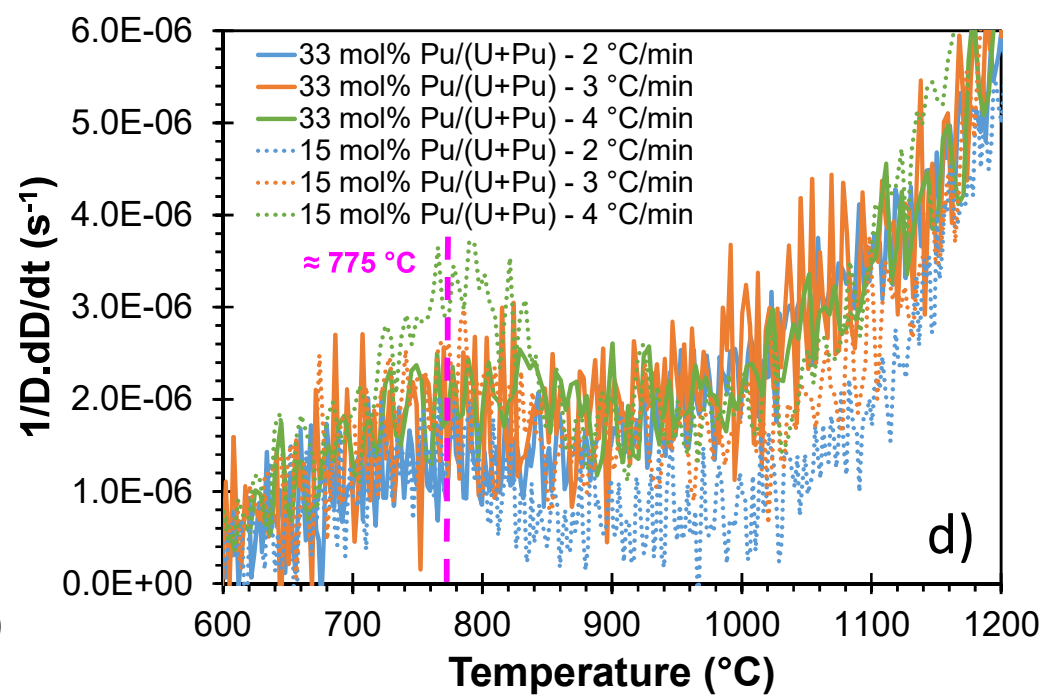
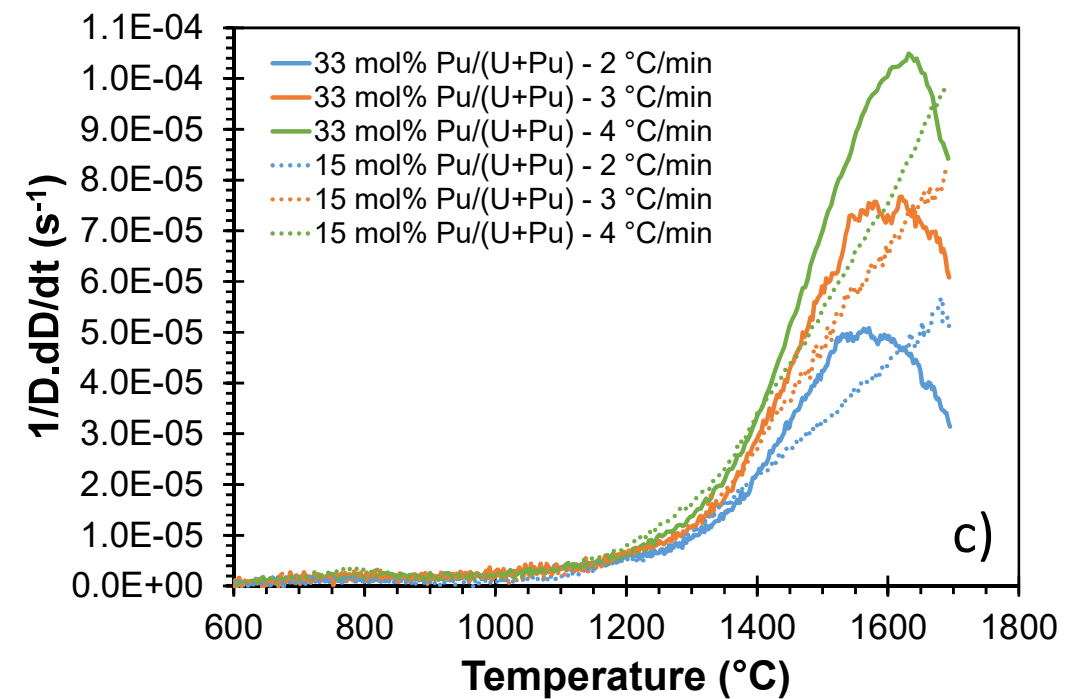
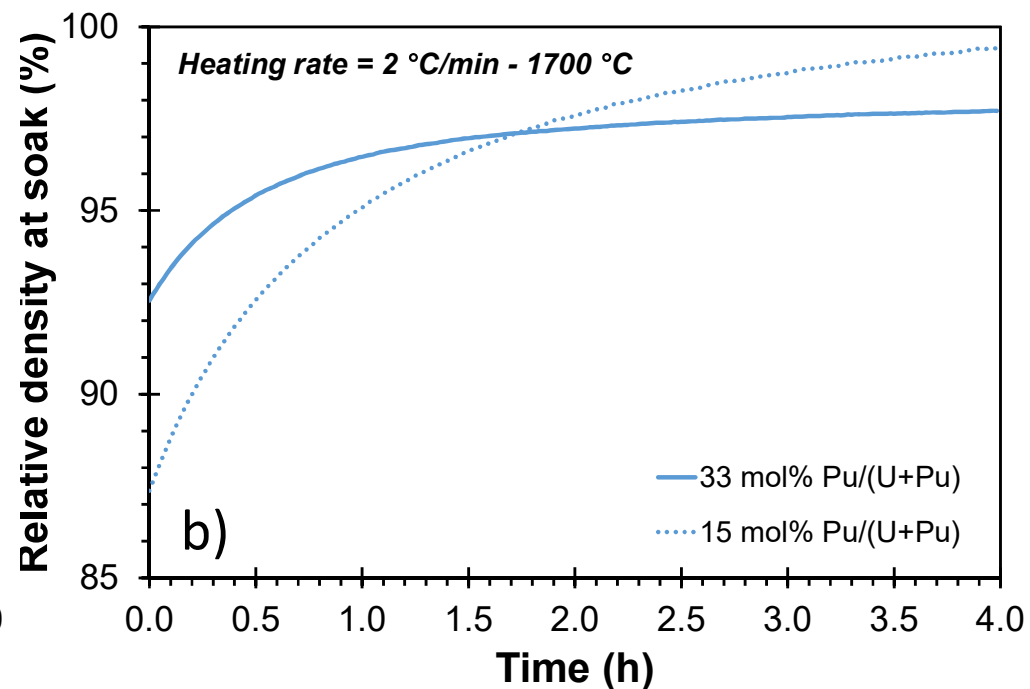
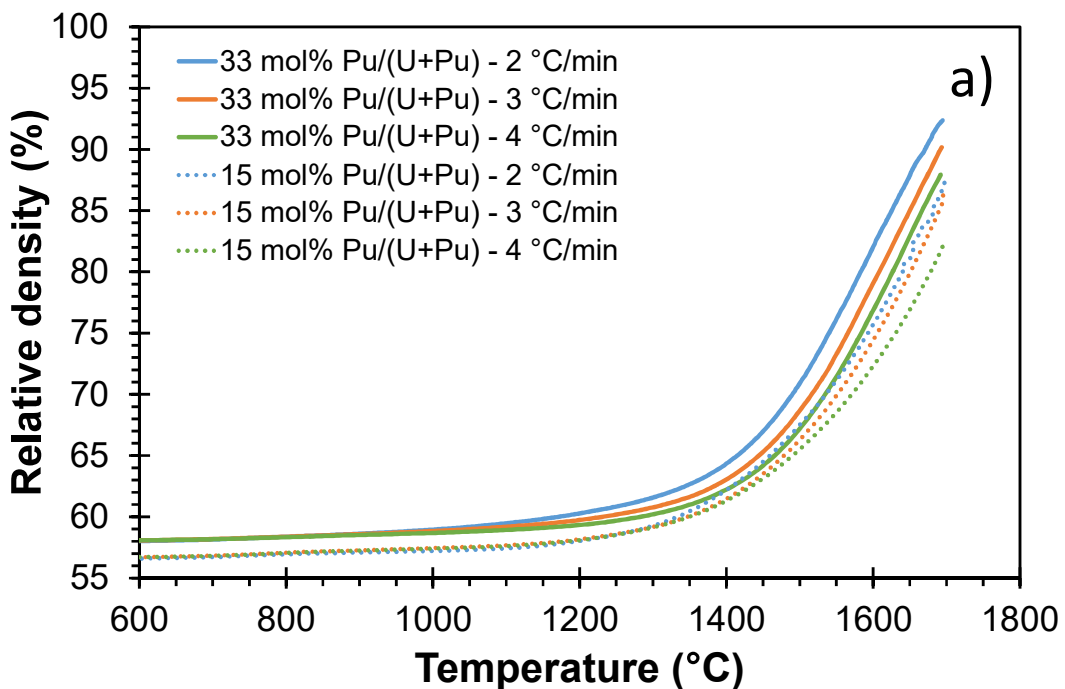
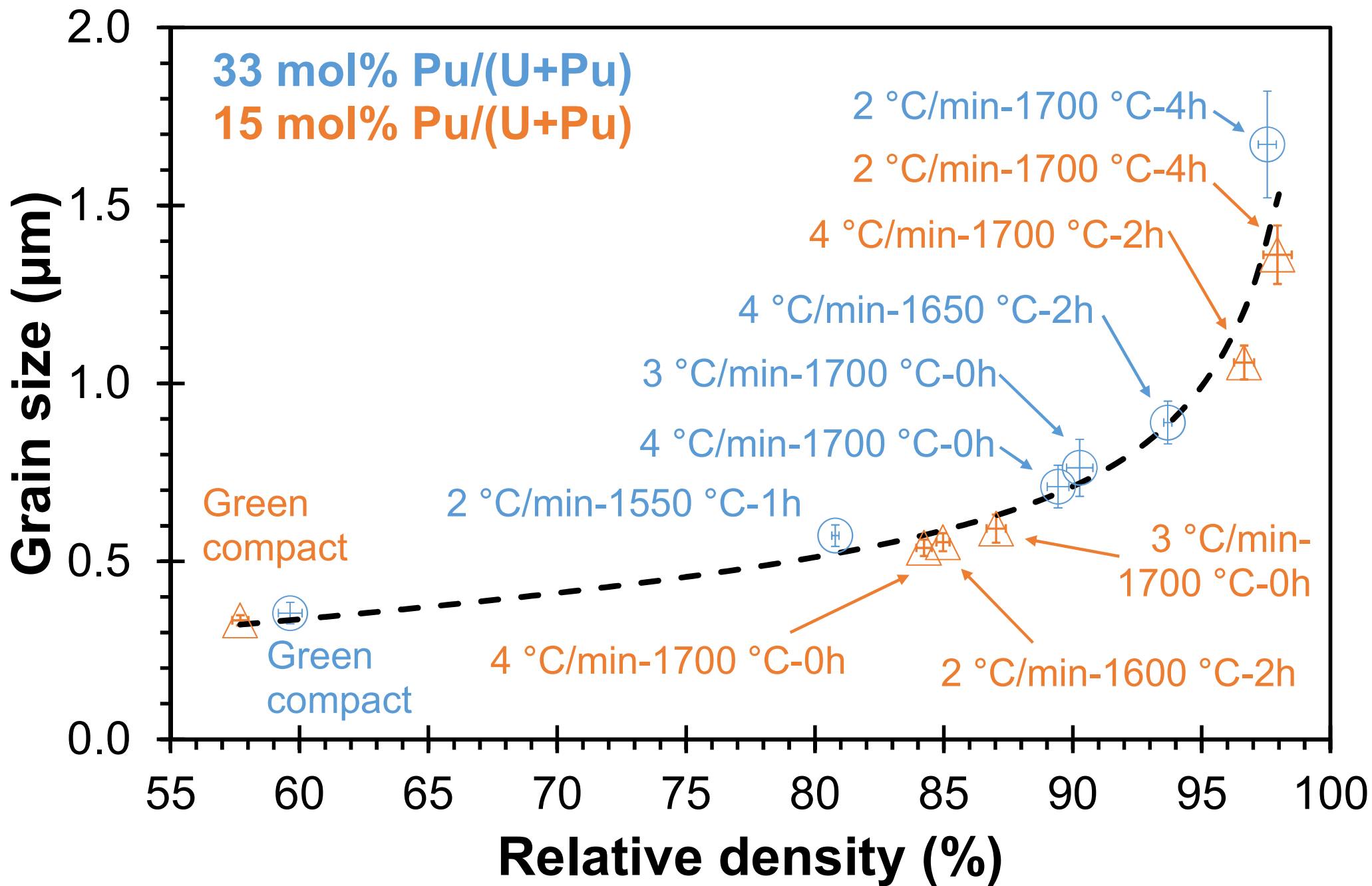
[Click here to access/download;Figure;Fig1.pptx](#)

Figure 2



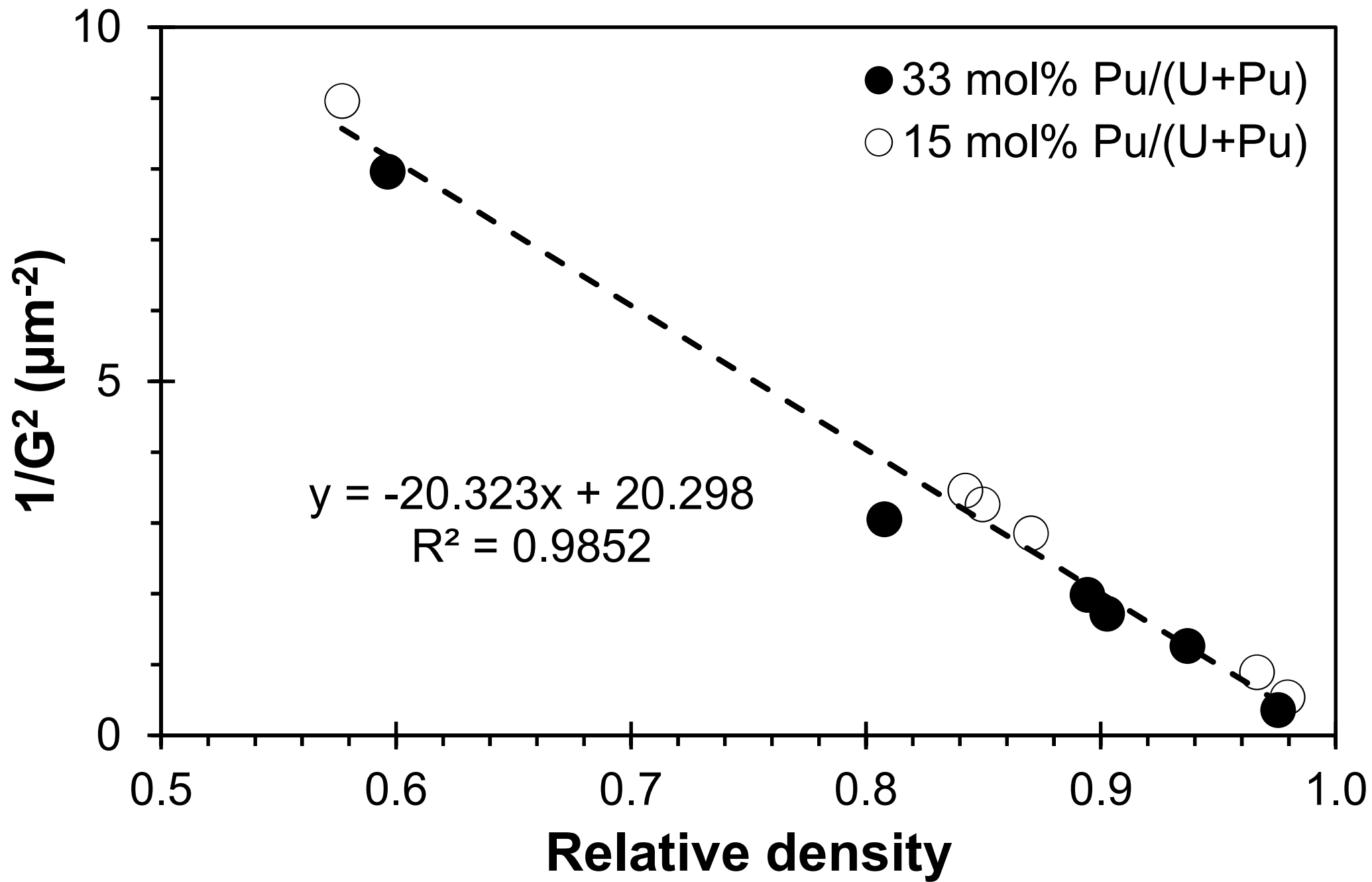


Figure 4

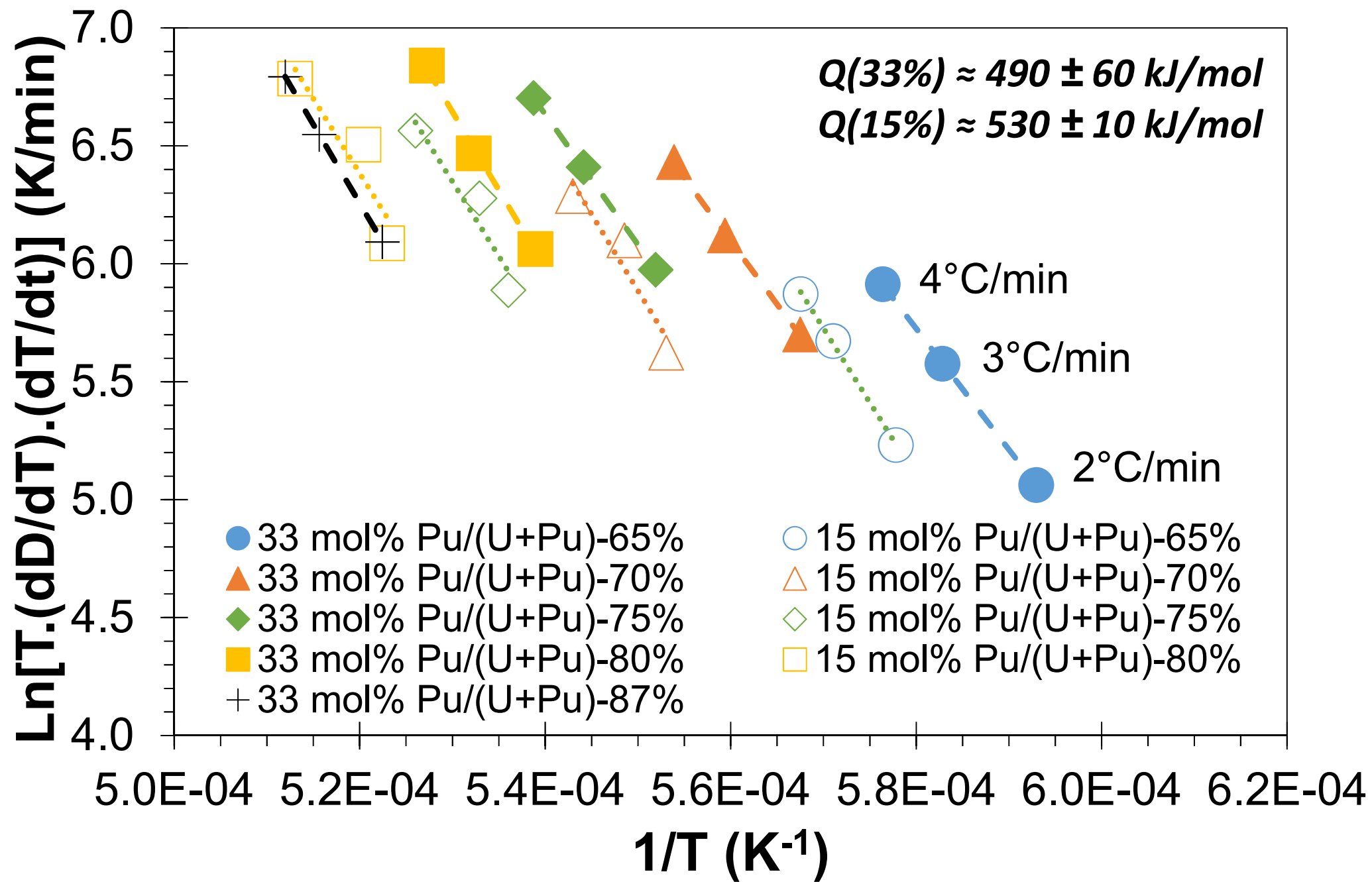


Figure 5

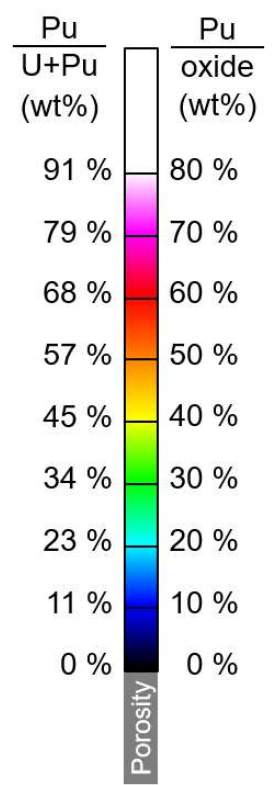
[Click here to access/download:Figure:Fig5.pptx](#)

Pu-M_β map

D = 97.6% - G = 1.67 μm
33 mol% Pu/(U+Pu)

15 mol% Pu/(U+Pu)
D = 97.9% - G = 1.36 μm

Pu-M_β map



200 μm

200 μm

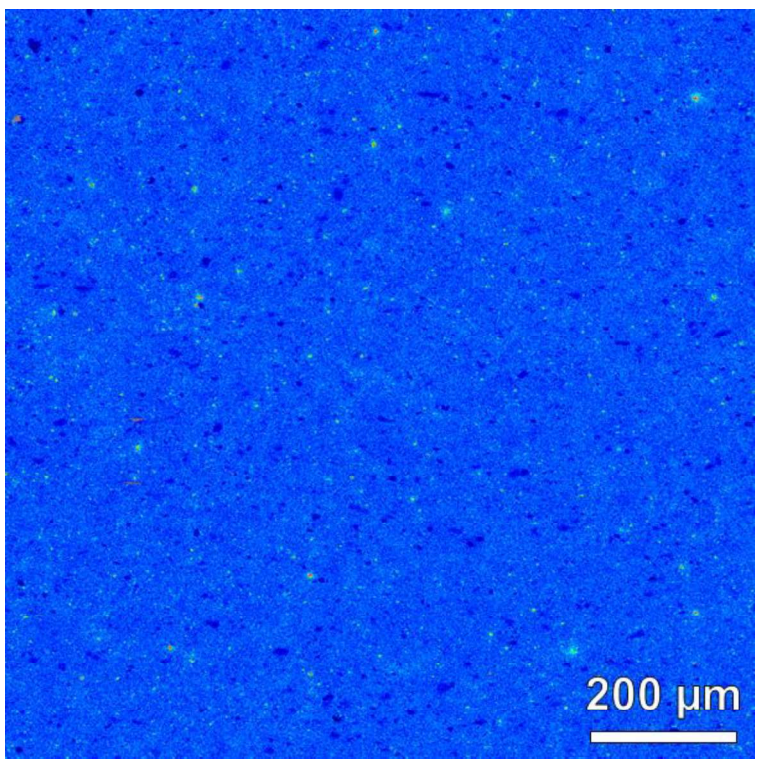
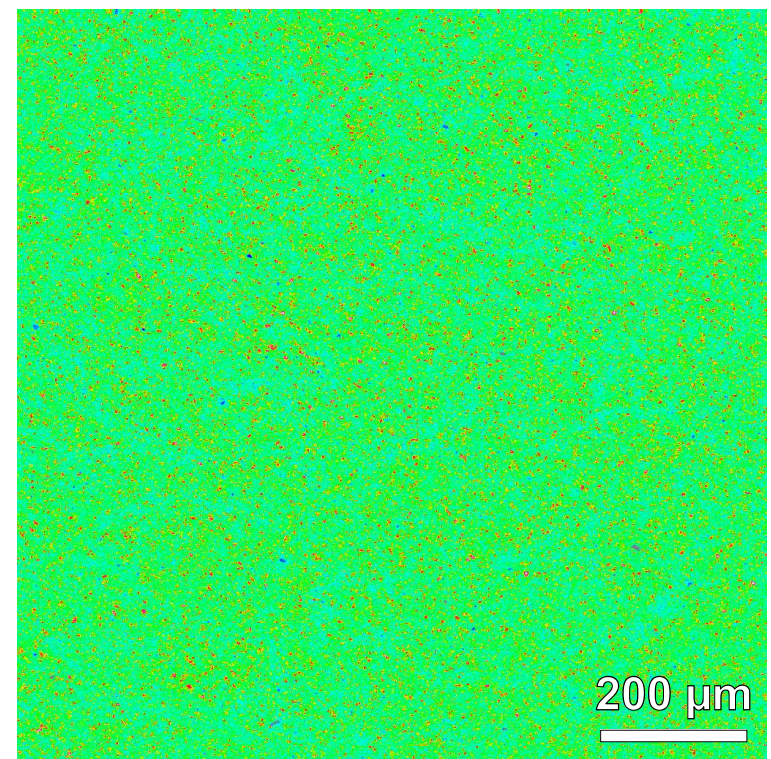
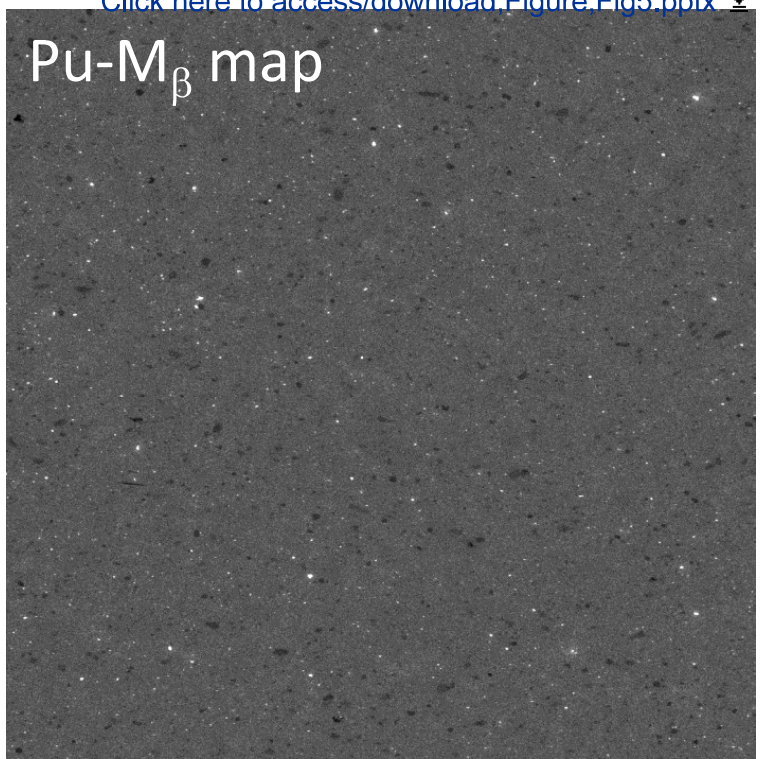
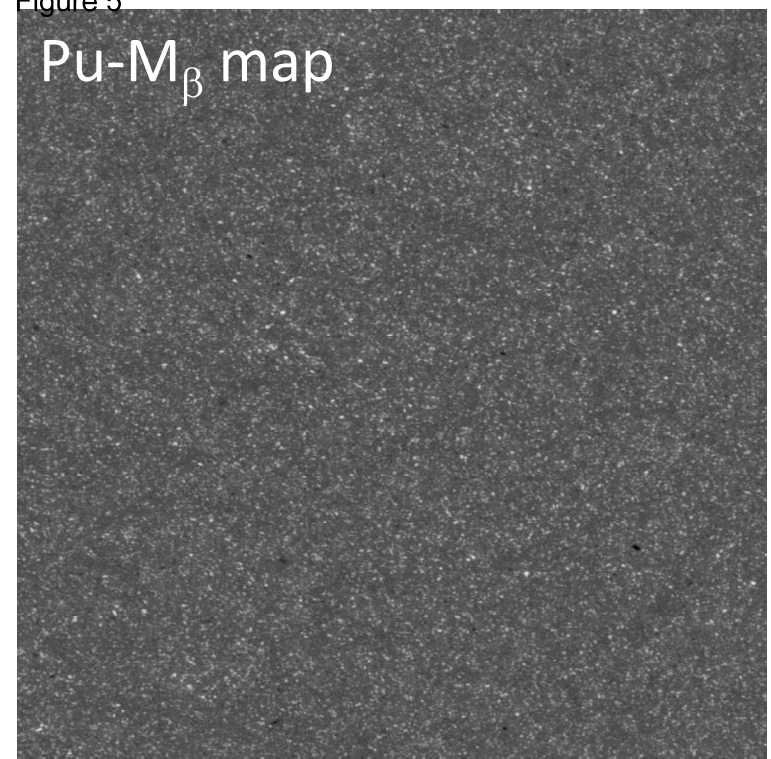


Figure captions

1
2
3
4 Fig. 1: a) Relative density as a function of the temperature during the heating
5 step; b) Relative density as a function of the soak time at 1700 °C; c)
6
7
8
9
10
11
12
13
14
15
16
17
18
19
20
21
22
23
24
25
26
27
28
29
30
31
32
33
34
35
36
37
38
39
40
41
42
43
44
45
46
47
48
49
50
51
52
53
54
55
56
57
58
59
60
61
62
63
64
65

Densification rate as a function of the temperature; d) zoom of c) in the 600-1200 °C temperature range

Fig. 2: Grain size versus relative density trajectory. For each experimental point, the values given are the heating rate, the sintering temperature and the time spent at the sintering temperature

Fig. 3: Fitting of the experimental points of the grain size versus relative density trajectory for a scenario based on densification being controlled by grain boundary diffusion and grain growth by the grain boundaries

Fig. 4: Determination of the apparent activation energy for densification using the anisothermal Constant Rates of Heating method. For each dataset, the value given is the density at which the data was extracted from the three heating rate values

Fig. 5: Pu-M_β intensity mapping obtained by EPMA/WDS at 20 kV (arbitrary grey scales) and coloured pseudo-quantified Pu mapping for 98% dense samples having similar grain sizes

Supplementary material: a) SEM observations of some typical granules constituting the freeze-granulated powders containing 33 and 15 mol% Pu/(U+Pu); b) Cumulative number frequency of the individual granules constituting the freeze-granulated powders containing 33 and 15 mol% Pu/(U+Pu). The measurements were performed using optical microscopy observations of powder samples positioned on a glass coverslip. Each individual

granule projected area is measured and an equivalent two-dimensional disc diameter is calculated (no correction factor). Around 1000 granules are considered for each powder

1
2
3
4
5
6
7
8
9
10
11
12
13
14
15
16
17
18
19
20
21
22
23
24
25
26
27
28
29
30
31
32
33
34
35
36
37
38
39
40
41
42
43
44
45
46
47
48
49
50
51
52
53
54
55
56
57
58
59
60
61
62
63
64
65